Single-crystal compression and crystal structure of clinopyroxene up to 10 GPa

LI ZHANG, HANS AHSBAHS, STEFAN S. HAFNER, AND ALI KUTOGLU

Scientific Center of Materials Sciences and Institute of Mineralogy, University of Marburg, 35032 Marburg, Germany

ABSTRACT

The hydrostatic compression of synthetic single crystals of diopside, $CaMgSi_2O_6$, and hedenbergite, $CaFeSi_2O_6$, was studied at 33 pressures up to 10 GPa by X-ray diffraction. In addition, intensity data for hedenbergite were collected at 12 pressures up to 10 GPa. For determination of the elasticity two crystals were loaded together in a diamond cell. The axial compressibilities β_a, β_b, and β_c of diopside and hedenbergite are 2.36(4), 3.17(4), and 2.50(4) $\times$ 10^{-3} GPa^{-1}, and 1.93(5), 3.38(6), and 2.42(8) $\times$ 10^{-3} GPa^{-1}, respectively. The bulk moduli (K_{T_0}) and their pressure derivatives (K'_{T_0}) were determined simultaneously from a weighted linear fit of a third order Birch-Murnaghan equation of state to the volume data at elevated pressures. K_{T_0} and K'_{T_0} are 104.1(9) GPa and 6.2(3) for diopside and 117(1) GPa and 4.3(4) for hedenbergite, respectively.

The unit-cell parameters decrease continuously with pressure. The larger polyhedra show more compression than the smaller ones. Between 0.1 MPa and 10 GPa the polyhedral volumes of CaO_8, FeO_6, and SiO_4 decrease by 8.4, 6.6, and 2.9%, respectively. The longest bonds of CaO_8 and FeO_6 show most compression. Significant compression in the two shortest Si-O1 and Si-O2 bond lengths of the SiO_4 tetrahedra was observed at relatively low pressures, resulting in a tetrahedral volume compression of 1.6% between 0.1 GPa and 4 GPa and 1.3% between 4 and 10 GPa. The compression of the unit cell can be described by the volume compression of the individual CaO_8 and FeO_6 polyhedra, with the SiO_4 tetrahedron playing a minor role. Diopside is more compressible than hedenbergite as shown by their axial and volume compressibilities because the FeO_6 octahedron is significantly more rigid than MgO_6 at high pressures. This observation implies that octahedrally coordinated Fe^{2+} behaves differently from Mg at high pressures, in contrast to their behavior at ambient conditions.

INTRODUCTION

Ca-rich clinopyroxenes are regarded as major minerals of the mantle models and they have been the subject of several recent studies (Levien et al. 1979; Levien and Prewitt 1981; Kandelin and Weidner 1988; Zhang et al. 1989; Zhang and Hafner 1992; Comodi et al. 1995). For example, significant amounts of Ca-rich clinopyroxenes are accounted for in both the pyrolite (Ringwood 1975) and piclogite (Anderson and Bass 1984) models, with a volume fraction ranging from about 10–40% in the upper mantle. One way to constrain these models tightly is to compare seismic velocities directly with sound velocities measured on mantle minerals in the laboratory under mantle pressures (Zhang and Chopelas 1994). To accomplish this, data are needed for precise determination of equations of state at high pressures.

Ca-rich clinopyroxenes have monoclinic symmetry (space group $C2/c$). Because of their low symmetry, it is not easy to obtain precise crystal structure data using high-pressure techniques on polycrystalline samples because of coincidence of equivlalent reflections and accidental overlap of nonequivalent reflections. Data now available were obtained mainly from single crystal dif-

fraction at high pressures (Levien and Prewitt 1981; Comodi et al. 1995). Because those experiments were limited to pressures up to about 5 GPa, it is necessary to measure data at higher pressures, considering the relatively small compressibility and relatively high structural freedom of clinopyroxene. Extended extrapolation of elasticity data, measured at relatively low pressures, to properties at high pressures in this case may yield large errors (Zeug et al. 1993).

Another interesting question is how cations such as Fe^{2+} and Mg influence the elasticity of Ca-rich clinopyroxenes at high pressures. Although such information is highly desirable in mantle modeling as well as for understanding the structure and dynamics of the Earth's mantle, it is not yet available, mainly for the following reasons: (1) difficulties in precise measurement of unit-cell parameters, (2) comparatively small compressibilities associated with comparatively large errors in the pressure determination (> 0.5% up to 10 GPa), and (3) complex substitution of cations in natural samples. To circumvent these problems in the present study, high-pressure single-crystal diffraction techniques were used to obtain precise unit-cell data. Synthetic end-member crystals of the bi-

nary system $Ca(Mg,Fe)Si_2O_6$ with well-defined cation occupancies were loaded together in one diamond cell assembly to compare distinct compressions between individual crystals without superposition of the additional error associated with independent pressure determinations. In this paper, we present single-crystal compressibility results for synthetic diopside, $CaMgSi_2O_6$, and hedenbergite, $CaFeSi_2O_6$, up to 10 GPa. We also present crystal structure data of hedenbergite up to 10 GPa. The equations of state of these minerals as well as the compression mechanisms of the crystal structures will be described.

Zhang and Hafner (1992) reported changes in the Fe^{2+} electronic state of Ca-rich clinopyroxenes shown by ^{57}Fe γ resonance experiments at high pressures. It is interesting to study the pressure dependence of these states and compare it with that of the Fe^{2+} polyhedral geometry, which determines the Fe-O bonding. Furthermore, Zhang and Hafner (1992) interpreted a discontinuity in ^{57}Fe hyperfine parameters of hedenbergite at 4 GPa as a phase transition. The data on Fe-O bond lengths at high pressures will allow correlated studies such as theoretical ab initio calculation to describe in detail the changes of Fe^{2+} electronic structure at high pressures, which are constrained by experimental data (Zhang and Hafner 1992).

EXPERIMENTAL DETAILS

Samples

Single crystals of hedenbergite, $CaFeSi_2O_6$, were synthesized in a belt apparatus at about 1150 °C and 4 GPa with an experiment time of 5.5 h. The crystals were transparent and yellowish- to brownish-green in color. Their chemical compositions were confirmed by electron microprobe analysis. Fe^{3+} in the samples could not be detected in ^{57}Fe Mössbauer spectra. Single crystals of diopside, $CaMgSi_2O_6$, were grown with the Czochralski method at about 1400 °C. The crystals were colorless. For the measurement of the unit-cell parameters a hedenbergite crystal with dimensions of about 80 × 64 × 48 μm and a diopside crystal of about 96 × 50 × 25 μm were used. For X-ray diffraction intensity measurements on hedenbergite, two polished crystals with dimensions of about 80 × 128 × 50 μm and 130 × 130 × 50 μm were used.

High-pressure X-ray diffraction technique

Unit-cell parameters at high pressure. A modified Merrill-Bassett four-screw diamond anvil cell was used. The diameter of the diamond culet was 600 μm. A gasket was machined from Thyrodur 2709 steel and preindented to about 80 μm with a 330 μm hole. After preindention and sample hole drilling, the gasket was hardened in an inert atmosphere or immersed in iron powder in a closed vessel at 500 °C without changing its surface characteristics and dimensions thereafter. This material allowed significantly larger sample thickness and larger sample hole at high pressures than the routinely used Inconel alloys. The hedenbergite and diopside crystals were loaded simultaneously in the same cell together with a ruby chip for pressure calibration. A 4:1 mixture of methanol to ethanol was used as the hydrostatic pressure-transmitting medium. Pressure was measured before and after each X-ray diffraction experiment using the pressure-induced shift of the R1 fluorescence line of ruby at hydrostatic pressure (Munro et al. 1985). The error of the pressure measurement was estimated to be 0.05 GPa. Typical halfwidths of reflections from hedenbergite as well as diopside were about 0.2° in ω. The measurements were completed with two consecutive mounts. For the first mount a broadening of the hedenbergite reflections from 0.2° to about 0.4° at 10 GPa was observed, while the reflections of diopside remained unbroadened, i.e., they remained the same as at ambient pressure. This suggests possible squeezing of the crystal between the two diamond anvils. This broadening disappeared by releasing pressure to about 7 GPa. This implies that the crystal was not crushed, consistent with optical observations under polarized transmitted light. This slight squeezing has little effect on the unit-cell parameters of hedenbergite measured at 10 GPa as demonstrated in Figure 1. The unit-cell parameters of each crystal were measured at 33 pressures on increasing as well as decreasing pressure.

Diffraction measurements were performed with a Stoe automated four circle diffractometer using MoKα radiation (0.7107 Å) monochromated by a graphite crystal. The diffractometer was operated at 55 kV and 35 mA. The unit-cell parameters were determined from up to 21 reflections with 2θ ranging from 13° to 39°. Each reflection was centered in eight positions (King and Finger 1979) to reduce zero and crystal-centering errors. The unit-cell parameters were calculated using the procedure of Ralph and Finger (1982). There was not any significant deviation between the unit-cell parameters constrained or not constrained to monoclinic symmetry in all the refinements. The results presented in this paper are constrained values.

Intensity measurement at high pressure. For intensity measurements on hedenbergite at high pressures, the same technique was employed as for unit-cell parameter measurements. A hemisphere of integrated intensities in reciprocal space 6° < 2θ < 60° at 11 different pressures up to 10 GPa was collected below the limiting value of $(\sin \theta)/\lambda = 0.7560$ Å^{-1}, whereas the integrated intensities at 4.2 GPa were collected below $(\sin \theta)/\lambda = 0.9044$ Å^{-1} in reciprocal space 6° < 2θ < 80°. The ω-scan width was 1.2° with a step size of 0.02°.

A specially designed collimator placed on the diffracted beam side of the diamond cell was used to reduce the background produced mainly by the beryllium backing plates of the diamond cell (Ahsbahs 1987). A reduction of the background up to a factor of 4 could be achieved in this way. For measuring the absorption that results primarily from the diamond anvils and the beryllium plates, a collimator with a diameter of 0.15 mm was used. The diameter of this beam was similar to that of the beams in the intensity collection procedure defined by the size of
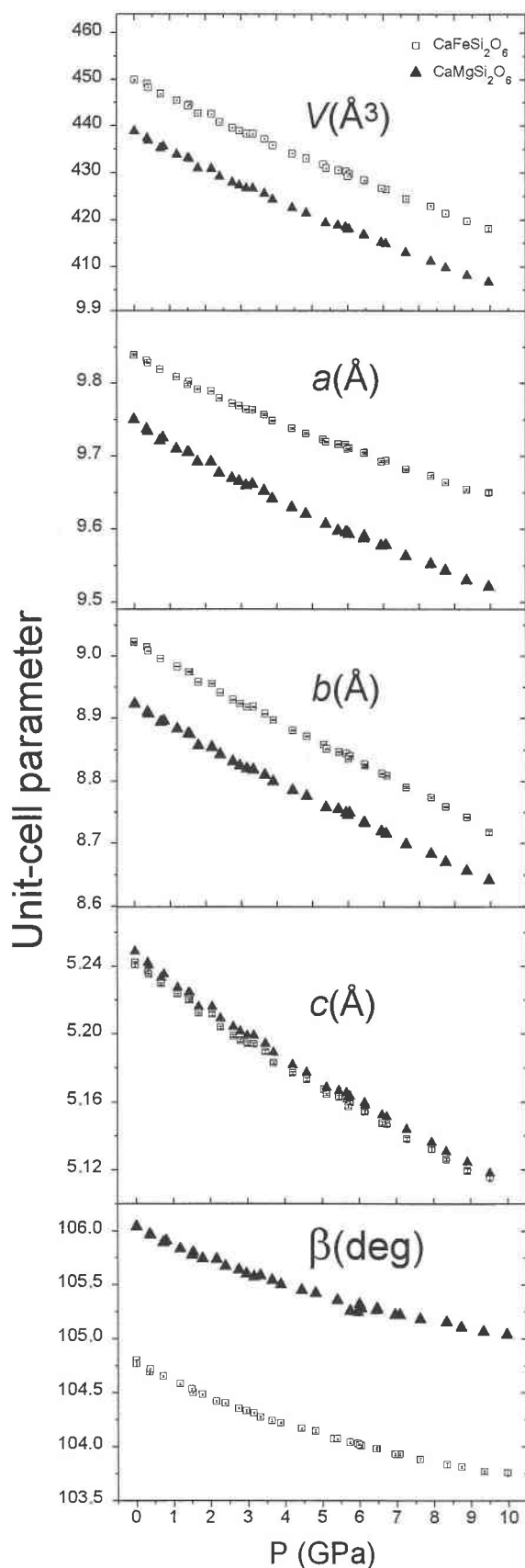
FIGURE 1. Unit-cell parameters of diopside and hedenbergite at 33 pressures. The standard deviations are generally smaller than data symbols.
←

the crystal. For absorption measurement this small-sized incident beam was adjusted to the center of the diamond culets of an empty cell without a gasket. The absorption curve, which depends on the tilting angle of the cell, was expressed analytically for the correction of the measured intensity.

It is known that the measured intensity of a reflection varies because of simultaneous reflection of the diamonds (Loveday et al. 1990). For our hedenbergite crystal the variation was as much as 25%. The width of the dips was about 1.5°. It was not easy to detect hedenbergite reflections, the intensity of which is weakened by simultaneous reflection of the diamonds. Because of the low crystal symmetry and the pressure cell geometry, most of the reflections can be measured only twice. We therefore adopted a procedure that helps to detect reflections weakened by simultaneous reflection: In a routine high pressure intensity measurement, the fixed-ϕ mode is usually used. For a reflection with its reflection position at $\chi = +90°$ or $\chi = -90°$, a rotation around ϕ is a rotation around the reflection vector (ψ scan) and this should not change the reflection intensity (Renninger effect ignored). If we make a series of intensity measurements on a reflection at different rotating angles around the reflection vector in a distance of more than 1.5° (typical width of a dip), it is possible to distinguish the intensities weakened by simultaneous reflections and approach statistically the real intensity. This, however, will not work for reflections with positions near $\chi = 0°$ or $\chi = 180°$. To circumvent this problem and to measure all accessible reflections at different ψ angles, we adopted the following procedure: First, the reflections in reciprocal space between $+45° < \chi < +135°$ and $-135° < \chi < -45°$ were measured at five different fixed-ϕ angles with steps of 1.8°. This resulted in four steps of 1.8° for reflections with $\chi \approx 90°$ and of 1.3° for those with $\chi \approx 45°$. Subsequently, the pressure cell was manually rotated relative to its fixing mount by 90° around the axis of the χ circle and the other half of the reflections were measured in the same way. This worked reasonably well for detecting affected intensities, especially those of strong reflections. By using the same weighting scheme, $1/\sigma^2_I$, in the least squares refinement, the weighted R values were reduced significantly compared to the measurements without using the above procedure (Table 1). The detection of damaged intensities for reflections with relatively weak intensities remained, however, difficult even by using this procedure. This is demonstrated by the deteriorated goodness-of-fit values for measurements, in which the above procedure was applied. This can be attributed to the different data quality

TABLE 1. Intensity measurement parameters for hedenbergite at various pressures

P (GPa)	Weights						Reflections			
	$1/\sigma_I^2$			$1/(\sigma_I^2 + cF^2)$*			Total	After averaging	Used for refinement	$I > 3\sigma$
	R_w	R	GOF	R_w	R	GOF				
0.0	1.81	3.02	2.07	3.20	2.94	1.13	840	377	334	275
1.1	1.78	3.29	2.15	3.20	3.17	1.12	913	422	372	288
2.1	2.13	4.00	2.41	4.33	3.83	1.23	916	418	370	297
2.8	1.76	3.17	2.68	2.95	3.06	1.71	1356	410	373	309
3.6	2.13	3.57	2.49	3.66	3.43	1.29	906	404	364	301
4.2	1.93	3.87	2.52	3.44	3.70	1.28	912	349	408	324
4.6	2.06	3.43	2.62	3.21	3.33	1.22	918	354	318	258
5.3**	1.33	3.30	3.26	2.73	2.90	1.06	4444	349	324	269
6.3**	1.33	3.15	3.18	2.97	2.89	1.15	4275	346	313	261
7.6**	1.34	3.06	3.27	2.75	2.74	1.08	4177	347	322	269
8.7**	1.35	2.87	2.98	2.62	2.53	1.04	4187	343	311	265
9.9**	1.38	2.65	3.32	2.51	2.30	1.00	4138	342	319	268

* Refined by SHELX76.
** Intensity data collected using the procedure of measuring every reflection at different ψ angles.

of strong and weak reflections. Further work is needed to circumvent this problem.

All data for the hedenbergite were collected with the crystal in the diamond cell. For data collection from 0–4.6 GPa the constant-precision mode was used with a maximum counting time per step of 8 s for $I/\sigma_I > 20$ (0, 1.0, and 2.1 GPa) and $I/\sigma_I > 40$ (2.8, 3.6, 4.2, 4.4, and 4.6 GPa). Above 5.3 GPa the procedure of rotating around the reflection vector was used for data collections with counting times of 1 s per step. No significant drift could be detected by monitoring the intensity of standard reflections every 2 h. Profiles of several reflections were scanned at each pressure to confirm hydrostatic pressure and crystal perfection. Further experiments were stopped because raising the pressure to 11.4 GPa caused a significant broadening of reflections that suggested a nonhydrostatic pressure.

For data reduction and structural refinements we used the program package CRYMIS (Kutoglu 1995). The observed integrated intensities were calculated according to Lehmann and Larsen (1974), and were corrected for absorption by the diamonds and beryllium backing plates. The intensities of the symmetrically equivalent reflections were averaged in Laue group 2/m, yielding between 311 and 408 reflections for the data sets at different pressures. In the data sets above 5.3 GPa, reflections, the intensities of which deviated more than $35\sigma_I$ from their averaged values, were excluded in the averaging procedure. The intensities were corrected for Lorenz and polarization effects. No correction for absorption by the crystal was applied to the intensities. Neutral atomic scattering factors of the *International Tables for X-ray Crystallography* (Ibers and Hamilton 1974) were used in the structure refinements. The initial atomic position parameters were obtained from Cameron et al. (1973). The refined parameters included a linear scaling factor, an isotropic

TABLE 2. Positional and isotropic displacement parameters of hedenbergite at high pressures

P (GPa)		0.0	1.1	2.1	2.8	3.6	4.2
Ca	y	0.29953(19)	0.30040(19)	0.30118(24)	0.30114(18)	0.30210(19)	0.30236(11)
	B*	0.68(3)	0.68(2)	0.66(3)	0.55(2)	0.56(3)	0.55(2)
Fe	y	0.90720(14)	0.90764(13)	0.90829(16)	0.90831(13)	0.90860(14)	0.90902(8)
	B	0.44(2)	0.47(2)	0.44(2)	0.45(2)	0.45(2)	0.40(2)
Si	x	0.28784(14)	0.28782(13)	0.28800(17)	0.28797(14)	0.28768(15)	0.28771(2)
	y	0.092495(18)	0.09305(17)	0.09319(22)	0.09355(17)	0.09394(18)	0.09362(10)
	z	0.23270(19)	0.23216(18)	0.23188(2)	0.23180(17)	0.23127(20)	0.23116(19)
	B	0.44(2)	0.43(2)	0.43(3)	0.43(2)	0.41(2)	0.42(2)
O1	x	0.11965(37)	0.11951(35)	0.12013(45)	0.12006(36)	0.11987(41)	0.12010(54)
	y	0.08995(44)	0.09068(44)	0.09058(53)	0.09073(45)	0.09107(44)	0.09112(25)
	z	0.15206(51)	0.15267(47)	0.15349(61)	0.15283(45)	0.15330(53)	0.15252(48)
	B	0.56(5)	0.57(5)	0.58(6)	0.65(5)	0.69(5)	0.65(4)
O2	x	0.36290(36)	0.36247(35)	0.36220(44)	0.36200(37)	0.36200(41)	0.36106(49)
	y	0.24596(45)	0.24747(44)	0.24791(54)	0.24830(44)	0.24843(51)	0.24851(28)
	z	0.32346(50)	0.32409(51)	0.32470(65)	0.32479(49)	0.32509(58)	0.32682(48)
	B	0.81(6)	0.88(6)	0.88(7)	0.84(6)	0.91(6)	0.70(5)
O3	x	0.35022(37)	0.35052(36)	0.35093(44)	0.35139(37)	0.35217(42)	0.35240(52)
	y	0.01994(40)	0.02100(42)	0.02114(51)	0.02186(39)	0.02278(44)	0.02332(26)
	z	0.99292(53)	0.99087(52)	0.98950(66)	0.98851(49)	0.98826(58)	0.98737(51)
	B	0.66(5)	0.70(5)	0.63(6)	0.55(5)	0.60(5)	0.68(4)

* Equivalent isotropic displacement parameter (Å^2).

secondary extinction factor, and positional and isotropic displacement parameters for each atom. The structure factors, F, were weighted according to $1/(\sigma_I^2 + cF2)$, where σ_I was calculated from counting statistics and c was refined from SHELX76. The reflections that obviously overlapped with diamond reflections were rejected in the refinements. The refinement conditions and the refined parameters are included in Tables 1 and 2. The observed and calculated structure factors are listed in Table 3.[1]

RESULTS

Our present study includes data on the unit-cell parameters of diopside and hedenbergite at pressures up to 10 GPa as well as data on the crystal structure of hedenbergite at 12 pressures between 0.1 MPa and 10 GPa. Unit-cell parameters of diopside up to 5.3 GPa and of hedenbergite up to 5.0 GPa were reported by Levien and Prewitt (1981) and Zhang et al. (1989), respectively. Levien and Prewitt (1981) also determined the crystal structure of diopside at pressures up to 5.3 GPa, whereas previous structure determinations of hedenbergite at high pressures are not known to us.

Axial compressibilities of diopside and hedenbergite

Unit-cell parameters of diopside and hedenbergite determined at 33 pressures between 0.1MPa to 10 GPa are presented in Tables 4 and 5 and Figure 1. The data measured in the diamond cell at ambient conditions are comparable with data published previously by Cameron et al. (1973). At high pressures the parameters decrease continuously with increasing pressure. No discontinuity could be detected within the experimental error. Our diopside

[1] A copy of Table 3 may be ordered as Document AM-97-634 from the Business Office, Mineralogical Society of America, 1015 Eighteenth Street, NW, Suite 601, Washington, DC 20036, U.S.A. Please remit $5.00 in advance for the microfiche.

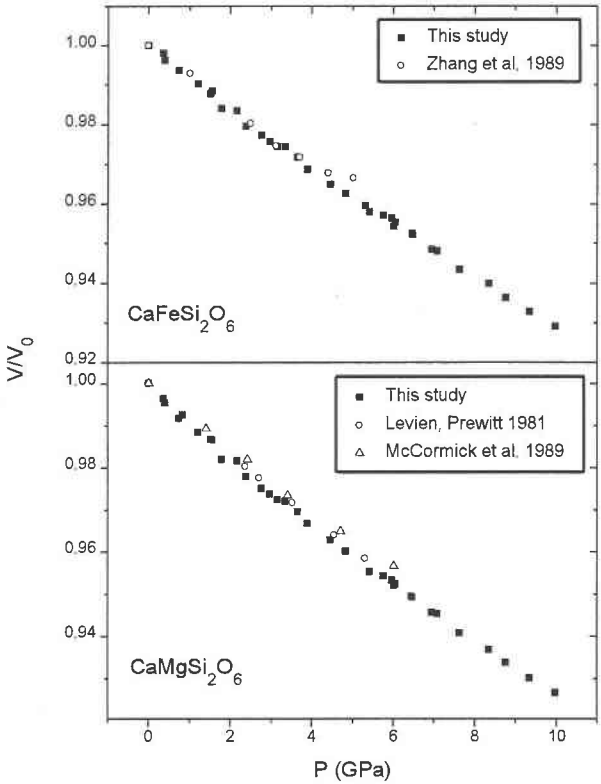**TABLE 4.** Unit-cell parameters of diopside between 0.1 MPa and 10 GPa

P (GPa)	a (Å)	b (Å)	c (Å)	β (°)	V (Å³)
0.0	9.749(2)	8.922(1)	5.2480(8)	106.04(1)	438.82(11)
0.36	9.736(2)	8.909(1)	5.2420(9)	105.96(1)	437.22(11)
0.38	9.7330(6)	8.907(1)	5.2402(5)	105.961(5)	436.82(6)
0.73	9.719(2)	8.892(1)	5.2360(4)	105.902(9)	435.20(10)
0.81	9.7200(9)	8.8920(8)	5.2370(4)	105.910(7)	435.37(6)
1.19	9.7090(7)	8.882(1)	5.2271(6)	105.833(6)	433.70(7)
1.50	9.7042(4)	8.8749(8)	5.2242(4)	105.771(4)	432.99(5)
1.53	9.704(2)	8.873(1)	5.2240(9)	105.80(1)	432.88(11)
1.78	9.6907(8)	8.856(1)	5.2158(7)	105.739(7)	430.85(8)
2.15	9.691(2)	8.852(2)	5.215(1)	105.73(2)	430.70(12)
2.38	9.6758(9)	8.841(1)	5.2087(7)	105.667(7)	429.07(8)
2.75	9.6688(9)	8.833(2)	5.2042(7)	105.630(7)	428.06(8)
2.95	9.6638(9)	8.824(1)	5.2013(6)	105.597(6)	427.23(7)
3.15	9.6586(7)	8.82(1)	5.1988(6)	105.573(6)	426.65(6)
3.33	9.659(2)	8.817(2)	5.198(1)	105.58(2)	426.54(13)
3.65	9.651(2)	8.808(2)	5.194(1)	105.54(2)	425.44(12)
3.88	9.640(1)	8.799(2)	5.1889(8)	105.501(8)	424.18(9)
4.44	9.628(1)	8.784(2)	5.1814(8)	105.446(8)	422.44(9)
4.83	9.620(1)	8.775(2)	5.1767(9)	105.416(9)	421.30(10)
5.40	9.6059(6)	8.756(1)	5.1681(5)	105.353(5)	419.20(6)
5.74	9.596(4)	8.754(4)	5.166(2)	105.25(3)	418.72(25)
5.95	9.594(4)	8.748(3)	5.165(2)	105.24(3)	418.33(22)
6.00	9.5947(9)	8.745(1)	5.1623(7)	105.314(8)	417.77(8)
6.04	9.592(2)	8.748(2)	5.162(1)	105.27(2)	417.95(14)
6.45	9.586(2)	8.732(1)	5.1580(9)	105.26(1)	416.65(10)
6.47	9.588(2)	8.732(1)	5.1570(9)	105.26(1)	416.65(10)
6.95	9.576(2)	8.718(2)	5.151(1)	105.22(2)	415.03(11)
7.08	9.577(2)	8.714(2)	5.150(1)	105.21(2)	414.84(13)
7.63	9.562(2)	8.697(2)	5.143(1)	105.17(2)	412.87(11)
8.35	9.551(2)	8.682(1)	5.1359(9)	105.14(1)	411.13(10)
8.75	9.543(2)	8.669(1)	5.130(1)	105.09(1)	409.79(10)
9.34	9.529(2)	8.655(1)	5.1240(9)	105.06(1)	408.15(10)
9.97	9.520(1)	8.640(1)	5.1180(7)	105.03(1)	406.62(8)

Note: Standard deviations in the last decimal digit are given in parentheses.

TABLE 2—*Continued*

P (GPa)		4.6	5.3	6.3	7.6	8.7	9.9
Ca	y	0.302 79(14)	0.30307(11)	0.30336(12)	0.30423(11)	0.30447(10)	0.30506(10)
	B^*	0.53(2)	0.50(2)	0.55(2)	0.50(2)	0.52(2)	0.53(2)
Fe	y	0.909 18(10)	0.90937(8)	0.909 72(8)	0.90987(7)	0.91001(7)	0.91031(7)
	B	0.38(2)	0.39(2)	0.41(2)	0.39(2)	0.41(2)	0.42(1)
Si	x	0.287 80(24)	0.28772(20)	0.287 56(21)	0.28779(20)	0.28793(19)	0.28757(17)
	y	0.093 64(12)	0.09392(10)	0.094 256(11)	0.09454(10)	0.09474(9)	0.09506(9)
	z	0.230 83(22)	0.23071(18)	0.23086(21)	0.23074(19)	0.23087(18)	0.23088(17)
	B	0.42(2)	0.37(2)	0.44(2)	0.38(2)	0.39(2)	0.39(2)
O1	x	0.120 64(59)	0.12070(51)	0.119 43(51)	0.11919(50)	0.12003(47)	0.11951(43)
	y	0.091 06(30)	0.09143(24)	0.09205(25)	0.09226(23)	0.09248(23)	0.09289(21)
	z	0.152 89(53)	0.15140(47)	0.15201(52)	0.15276(47)	0.15227(45)	0.15248(42)
	B	0.59(5)	0.64(4)	0.58(5)	0.63(4)	0.62(4)	0.61(4)
O2	x	0.361 07(56)	0.36140(51)	0.361 40(49)	0.36074(47)	0.35991(45)	0.35991(40)
	y	0.249 28(36)	0.25005(28)	0.25068(30)	0.25155(27)	0.25203(27)	0.25266(24)
	z	0.326 80(57)	0.32681(52)	0.32834(53)	0.32893(47)	0.32914(48)	0.33002(43)
	B	0.72(6)	0.71(4)	0.82(5)	0.78(5)	0.77(4)	0.74(4)
O3	x	0.351 93(61)	0.35300(52)	0.352 46(54)	0.35303(50)	0.35338(47)	0.35335(44)
	y	0.023 38(31)	0.02373(24)	0.02412(26)	0.02516(24)	0.02592(24)	0.02593(22)
	z	0.987 16(60)	0.98570(50)	0.98553(59)	0.98511(53)	0.98464(51)	0.98444(48)
	B	0.65(5)	0.59(4)	0.67(5)	0.63(4)	0.63(4)	0.62(4)

TABLE 5. Unit-cell parameters of hedenbergite between 0.1 MPa and 10 GPa

P (GPa)	a (Å)	b (Å)	c (Å)	β (°)	V (Å³)
0.0	9.8389(8)	9.0214(7)	5.2424(7)	104.797(8)	449.90(7)
0.0	9.838(2)	9.022(2)	5.241(2)	104.76(2)	449.88(15)
0.36	9.831(1)	9.014(1)	5.237(1)	104.69(1)	449.01(12)
0.38	9.8277(8)	9.0074(7)	5.2352(7)	104.717(8)	448.23(7)
0.73	9.8193(7)	8.9955(7)	5.2297(7)	104.650(7)	446.92(6)
1.19	9.8086(7)	8.9832(7)	5.2233(7)	104.579(7)	445.42(6)
1.50	9.797(1)	8.9742(8)	5.2201(7)	104.53(1)	444.31(8)
1.53	9.802(1)	8.975(1)	5.219(1)	104.50(1)	444.59(9)
1.78	9.7910(9)	8.9590(8)	5.2120(8)	104.481(9)	442.68(8)
2.15	9.789(1)	8.955(1)	5.211(1)	104.42(1)	442.48(9)
2.38	9.7793(9)	8.9413(8)	5.2039(8)	104.400(9)	440.73(8)
2.75	9.7722(9)	8.9307(8)	5.1989(8)	104.354(9)	439.56(8)
2.95	9.7684(9)	8.9240(8)	5.1963(8)	104.332(9)	438.88(7)
3.15	9.7639(9)	8.9185(8)	5.1943(8)	104.311(9)	438.28(8)
3.33	9.762(1)	8.918(1)	5.193(1)	104.27(1)	438.28(9)
3.65	9.756(1)	8.907(1)	5.189(1)	104.24(1)	437.16(10)
3.88	9.7498(9)	8.8981(8)	5.1839(8)	104.220(9)	435.95(8)
4.44	9.7378(9)	8.8806(8)	5.1767(8)	104.166(9)	434.06(7)
4.83	9.731(1)	8.870(1)	5.172(1)	104.14(1)	433.01(9)
5.30	9.722(1)	8.858(1)	5.167(1)	104.07(1)	431.69(9)
5.40	9.7194(8)	8.8518(7)	5.1642(7)	104.069(8)	430.97(7)
5.74	9.716(1)	8.847(1)	5.1620(9)	104.03(1)	430.54(9)
5.95	9.715(2)	8.843(1)	5.161(1)	104.02(2)	430.24(13)
6.00	9.709(1)	8.8358(8)	5.1572(8)	104.01(1)	429.26(8)
6.04	9.710(1)	8.840(1)	5.159(1)	104.01(1)	429.74(9)
6.45	9.704(1)	8.827(1)	5.153(1)	103.98(1)	428.44(9)
6.47	9.704(2)	8.825(2)	5.153(2)	103.97(2)	428.35(15)
6.95	9.692(1)	8.8110(9)	5.147(1)	103.92(1)	426.70(9)
7.08	9.693(1)	8.809(1)	5.146(1)	103.93(1)	426.52(9)
7.63	9.680(1)	8.789(1)	5.138(1)	103.87(1)	424.49(10)
8.35	9.672(2)	8.774(2)	5.132(2)	103.83(2)	422.90(12)
8.75	9.663(1)	8.7580(9)	5.1250(9)	103.80(1)	421.31(8)
9.34	9.653(1)	8.742(1)	5.119(1)	103.76(1)	419.64(10)
9.97*	9.649(3)	8.717(3)	5.116(3)	103.76(3)	418.02(27)

Note: Standard deviations in the last decimal digit are given in parentheses.
* Slight squeezing observed.

FIGURE 2. Pressure dependence of the unit-cell volumes for diopside and hedenbergite

data between 0.1 MPa and 5.3 GPa agree with those of Levien and Prewitt (1981) as shown in Figure 2. They deviate, however, from the data of McCormick et al. (1989). McCormick et al. (1989) attributed this deviation to error in the pressure determination. The present single-crystal hedenbergite data agree well with those measured on a polycrystalline sample between 0.1 MPa and 3.7 GPa (Zhang et al. 1989). The data at 4.4 and 5.0 GPa obtained from the polycrystalline sample, however, show

a significant deviation from the present single-crystal data. This appears to result from nonhydrostatic pressure applied to the polycrystalline sample in the previous study.

The technique of loading several crystals together in the same diamond cell assembly (Hazen 1993) allows detection of very small differences of compression among crystals. This is especially useful for mantle minerals with comparably small compressibilities. Our data obtained by this technique show that both diopside and hedenbergite exhibit anisotropic compression. The axial compressibilities, β_a, β_b, and β_c, are 2.36(4), 3.17(4), and

TABLE 6. Bulk moduli (K_{T_0}) and their pressure derivatives (K'_{T_0}) of diopside and hedenbergite

Sample	K_{T_0} (GPa)	K'_{T_0}	P_{max}* (GPa)	Method	Reference
Diopside, SC**	112	—	0	Brillouin	Aleksandrov and Rythova (1961)
Diopside, SC	113	—	0	Brillouin	Levien et al. (1979)
Diopside, SC	114(4)	4.5(1.8)	5.3	X-ray	Levien and Prewitt (1981)
Diopside, SC	122(2)	4.0†	6.0	X-ray	McCormick et al. (1989)
Diopside, SC	104.1(9)	6.2(3)	10	X-ray	This study
Diopside	105	6.2	5	Simulation	Matsui and Busing (1984)
Hedenbergite, SC	120	—	0	Brillouin	Kandelin and Weidner (1988)
Hedenbergite, PC	119(2)	4.0†	3.7	X-ray	Zhang et al. (1989)
Hedenbergite, SC	117(1)	4.3(4)	10	X-ray	This study

Note: Standard deviations in the last decimal digit are given in parentheses.
* P_{max} = maximum pressure.
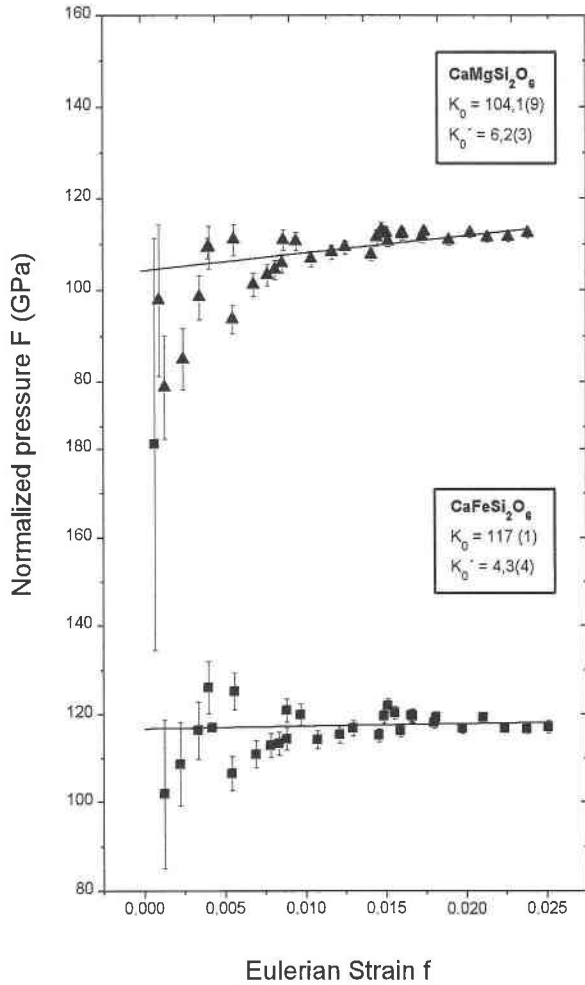** SC = single crystal; PC = polycrystalline sample.
† K'_{T_0} fixed at 4.

FIGURE 3. Eulerian strain (f) versus the Birch normalized stress (F). Solid lines are the weighted linear regressions to F-f data points.

2.50(4) × 10⁻³ GPa⁻¹ for diopside, and 1.93(5), 3.38(6), and 2.42(8) × 10⁻³ GPa⁻¹ for hedenbergite. The b axis is the most compressible direction. The compressions along the three crystallographic axes in both minerals follow the same trend. The difference in the compression of the a axis between diopside and hedenbergite, however, is about 20%.

Equations of state of diopside and hedenbergite

The isothermal bulk moduli K_T at zero pressure, K_{T_0}, and their first pressure derivatives K'_{T_0} may be derived by a third-order Birch-Murnaghan equation of state (Birch 1978) expressed in terms of the Eulerian strain, f, and the Birch normalized pressure, F,

$$F = K_{T_0} [1 + 1.5f(K'_{T_0} - 4)] \quad (1)$$
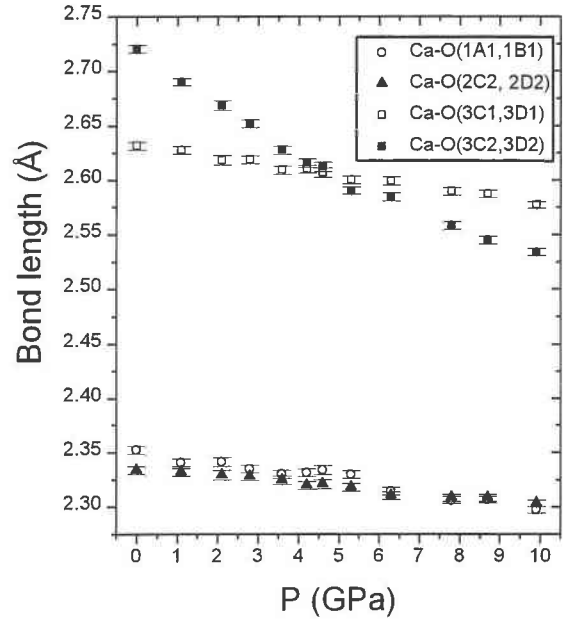
where

$$f = [(V/V_0)^{-2/3} - 1]/2 \quad (2)$$

and

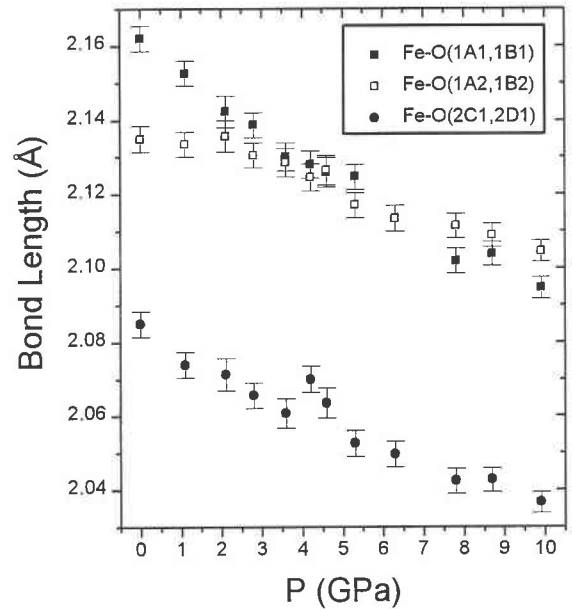FIGURE 4. Pressure dependence of Ca-O interatomic distances in the CaO₈ polyhedra.

FIGURE 5. Pressure dependence of Fe-O interatomic distances in the FeO₆ octahedra.

TABLE 7. Reuss and Voigt averages of diopside and hedenbergite

Average	CaMgSi₂O₆*	CaMgSi₂O₆**	CaFeSi₂O₆†
Reuss (GPa)	108(1)	105(4)	116.1
Voigt (GPa)	117(1)	118(4)	123.9

Note: Standard deviations in the last decimal digit are given in parentheses.
* Data from Levien and Prewitt (1979).
** Data from Aleksandrov et al. (1964).
† Data from Kandelin and Weidner (1988).

TABLE 8. Selected bond lengths (Å) and angles (°), polyhedral volume (Å³), and distortion parameters for the polyhedra in hedenbergite at high pressures

P (GPa)	0.00	1.1	2.1	2.8	3.6	4.2
			CaO₈ polyhedron			
Ca-O(1A1,B1) × 2	2.3518(36)	2.3403(35)	2.3407(43)	2.3342(35)	2.3293(38)	2.3308(36)
Ca-O(2C2,D2) × 2	2.3329(36)	2.3315(35)	2.3284(44)	2.3270(35)	2.3239(40)	2.3192(35)
Ca-O(3C1,D1) × 2	2.6316(35)	2.6270(35)	2.6176(43)	2.6181(34)	2.6086(38)	2.6092(36)
Ca-O(3C2,D2) × 2	2.7199(35)	2.6893(35)	2.6676(43)	2.6510(34)	2.6266(38)	2.6149(36)
Volume	26.02(5)	25.71(5)	25.46(5)	25.29(5)	25.00(5)	24.92(6)
			FeO₆ octahedron			
Fe-O(1A1,B1) × 2	2.1619(35)	2.1524(34)	2.1421(42)	2.1385(34)	2.1299(38)	2.1278(36)
Fe-O(1A2,B2) × 2	2.1348(35)	2.1333(34)	2.1355(42)	2.1303(34)	2.1283(38)	2.1244(36)
Fe-O(2C1,D1) × 2	2.0848(35)	2.0737(35)	2.0712(43)	2.0654(35)	2.0606(40)	2.0698(35)
Fe-Fe	3.1089(10)	3.0926(10)	3.0767(12)	3.0701(10)	3.0584(10)	3.0514(6)
O(1A1)-O(1B1)	2.797(5)	2.781(5)	2.778(4)	2.773(4)	2.759(5)	2.764(5)
O(2C1)-O(2D1)	2.987(5)	2.988(5)	2.987(6)	2.985(5)	2.978(5)	3.001(5)
O(1A1)-O(2C1) × 2	3.109(5)	2.926(5)	3.066(6)	3.061(5)	3.053(5)	3.053(5)
O(1A1)-O(1A2) × 2	3.082(5)	3.077(4)	3.071(6)	3.061(5)	3.055(5)	3.053(5)
O(1A2)-O(2C1) × 2	2.940(5)	2.926(5)	2.920(6)	2.910(5)	2.903(5)	2.906(5)
O(1A2)-O(2D1) × 2	3.052(5)	3.038(5)	3.038(6)	3.037(5)	3.024(5)	3.014(5)
O(1A1)-O(1B2) × 2	2.966(5)	2.967(5)	2.972(5)	2.966(5)	2.963(5)	2.962(5)
O(1A1)-Fe-O(1B1)	80.6(1)	80.5(1)	80.8(2)	80.9(1)	80.7(1)	81.0(1)
O(1A1)-Fe-O(1A2) × 2	91.6(1)	91.8(1)	91.6(2)	91.6(1)	91.7(1)	91.8(1)
O(1A1)-Fe-O(2C1) × 2	94.1(1)	93.8(1)	93.6(2)	93.5(1)	93.5(1)	93.2(1)
O(1A1)-Fe-O(1B2) × 2	87.3(1)	87.6(1)	88.0(2)	88.0(1)	88.2(1)	88.3(1)
O(1A2)-Fe-O(2C1) × 2	88.3(1)	88.1(1)	87.9(2)	87.8(1)	87.7(1)	87.7(1)
O(1A2)-Fe-O(2D1) × 2	92.6(1)	92.4(1)	92.5(2)	92.5(1)	92.4(1)	92.3(1)
O(2C1)-Fe-O(2D1)	91.5(1)	92.2(1)	92.3(2)	92.5(1)	92.5(2)	92.9(1)
Volume	12.75(2)	12.62(2)	12.56(3)	12.48(2)	12.39(2)	12.41(3)
⟨λ⟩	1.0045(23)	1.0045(23)	1.0041(28)	1.0042(27)	1.0042(20)	1.0040(14)
σ²	14.87	14.68	13.53	13.59	13.71	13.24
			SiO₄ tetrahedron			
SiO(1C1)	1.5992(37)	1.5978(36)	1.5902(45)	1.5889(16)	1.5853(39)	1.5819(38)
SiO(2C1)	1.5839(37)	1.5846(36)	1.5818(45)	1.5780(36)	1.5733(41)	1.5733(37)
Si-O(3C1)	1.6661(36)	1.6657(36)	1.6658(44)	1.6668(35)	1.6643(40)	1.6639(38)
Si-O(3C2)	1.6844(36)	1.6828(36)	1.6768(44)	1.6773(35)	1.6833(40)	1.6808(38)
Si-Si	3.1060(19)	3.0993(18)	3.0909(23)	3.0878(18)	3.0826(20)	3.0765(20)
O(1C1)-O(2C1)	2.7226(49)	2.7176(48)	2.7076(59)	2.7040(48)	2.6991(54)	2.6895(50)
O(1C1)-O(3C1)	2.6830(48)	2.6843(47)	2.6787(58)	2.6770(47)	2.6790(52)	2.6747(51)
O(1C1)-O(3C2)	2.6919(48)	2.6906(47)	2.6807(58)	2.6836(47)	2.6886(52)	2.6887(51)
O(2C1)-O(3C1)	2.6575(48)	2.6591(48)	2.6602(59)	2.6564(47)	2.6456(54)	2.6503(50)
O(2C1)-O(3C2)	2.5721(48)	2.5751(48)	2.5670(59)	2.5671(47)	2.5653(54)	2.5620(50)
O(3C1)-O(3C2)	2.6441(48)	2.6376(47)	2.6299(58)	2.6266(46)	2.6220(52)	2.6209(50)
O(1C1)-Si-O(2C1)	117.6(2)	117.3(2)	117.2(2)	117.3(2)	117.4(2)	116.9(2)
O(1C1)-Si-O(3C1)	110.5(2)	110.7(2)	110.7(2)	110.6(2)	111.0(2)	111.0(2)
O(1C1)-Si-O(3C2)	110.1(2)	110.2(2)	110.2(2)	110.5(2)	110.7(2)	111.0(2)
O(2C1)-Si-O(3C1)	109.7(2)	109.8(2)	110.0(2)	109.9(2)	109.6(2)	109.9(2)
O(2C1)-Si-O(3C2)	103.8(2)	104.0(2)	103.9(2)	104.1(2)	103.9(2)	103.8(2)
O(3C1)-Si-O(3C2)	104.2(2)	103.9(2)	103.8(2)	103.5(2)	103.1(2)	103.2(2)
Si-O3-Si	135.9(2)	135.5(2)	135.2(3)	134.8(2)	134.1(2)	133.8(2)
O3-O3-O3	164.4(2)	163.6(2)	163.5(2)	162.9(2)	162.2(2)	161.8(2)
Volume	2.218(7)	2.216(7)	2.199(9)	2.196(7)	2.189(8)	2.184(7)
[λ]	1.0061(23)	1.0059(22)	1.0060(28)	1.0061(29)	1.0062(26)	1.0062(30)
σ²	25.58	24.83	25.18	25.59	26.05	25.44
Tilting angle (°)*	3.07(9)	2.88(9)	2.71(11)	2.55(10)	2.36(10)	2.08(10)

Note: Standard deviations are given in parentheses.
* Angle between basal plane of a tetrahedron and the (100) plane.

$$F = P/[3f(1 + 2f)^{2.5}]. \qquad (3)$$

In Equations 1–3 P is the pressure, and V and V_0 are the molar volumes at high pressure and at ambient pressure, respectively.

The K_{T_0} and K'_{T_0} values were determined by a weighted linear least-squares fit to the f and F terms of Equations 1–3, using the unit-cell parameters of Tables 4 and 5. As is clear from Equation 1 the intercept of this fit at P = 0 is K_{T_0}, whereas the slope indicates the deviation of K'_{T_0}

from 4. The data in Figure 3 demonstrate a positive slope for diopside and a nearly zero slope for hedenbergite, corresponding to values of $K'_{T_0} = 6.2(3)$ for diopside and $K'_{T_0} = 4.3(4)$ for hedenbergite. The K_{T_0} and K'_{T_0} values obtained from this procedure are presented in Table 6. Comparison of K_{T_0} determined in this study with the adiabatic bulk modulus K_S derived from Voigt-Reuss-Hill averages by use of measurements at ambient conditions (Aleksandrov and Rythova 1961; Levien et al. 1979;

TABLE 8—*Continued*

P(GPa)	4.6	5.3	6.3	7.6	8.7	9.9
			CaO₈polyhedron			
Ca-O(1A1,B1) × 2	2.3331(41)	2.3288(35)	2.3138(35)	2.3057(34)	2.3061(32)	2.2969(29)
Ca-O(2C2,D2) × 2	2.3199(41)	2.3171(36)	2.3098(36)	2.3077(33)	2.3078(32)	2.3025(29)
Ca-O(3C1,D1) × 2	2.6060(42)	2.5992(35)	2.5982(38)	2.5888(35)	2.5864(33)	2.5763(31)
Ca-O(3C2,D2) × 2	2.6114(42)	2.5896(35)	2.5835(38)	2.5577(35)	2.5442(33)	2.5333(31)
Volume	24.92(6)	24.65(5)	24.45(5)	24.16(5)	24.08(4)	23.84(4)
			FeO₆octahedron			
Fe-O(1A1,B1) × 2	2.1258(40)	2.1245(34)	2.1133(35)	2.1018(33)	2.1037(32)	2.0945(29)
Fe-O(1A2,B2) × 2	2.1263(40)	2.1169(34)	2.1132(35)	2.1112(33)	2.1087(32)	2.1044(29)
Fe-O(2C1,D1) × 2	2.0634(41)	2.0524(36)	2.0495(35)	2.0422(33)	2.0426(32)	2.0365(29)
Fe-Fe	3.0462(7)	3.0368(5)	3.0274(6)	3.0148(5)	3.0073(5)	2.9960(5)
O(1A1)-O(1B1)	2.770(6)	2.773(5)	2.759(5)	2.723(5)	2.738(5)	2.721(4)
O(2C1)-O(2D1)	2.998(6)	2.985(5)	3.009(5)	2.993(5)	3.006(5)	3.004(4)
O(1A1)-O(2C1) × 2	3.036(6)	3.024(5)	3.018(5)	2.997(5)	2.987(5)	2.974(4)
O(1A1)-O(1A2) × 2	3.049(6)	3.044(5)	3.042(5)	3.035(5)	3.030(5)	3.026(4)
O(1A2)-O(2C1) × 2	2.899(6)	2.879(5)	2.888(5)	2.874(5)	2.864(5)	2.858(4)
O(1A2)-O(2D1) × 2	3.023(6)	3.010(5)	3.014(5)	2.982(5)	2.986(5)	2.972(4)
O(1A1)-O(1B2) × 2	2.967(6)	2.961(5)	2.964(5)	2.943(5)	2.950(5)	2.942(4)
O(1A1)-Fe-O(1B1)	81.3(2)	81.5(1)	81.3(1)	80.7(1)	81.2(1)	81.0(1)
O(1A1)-Fe-O(1A2) × 2	91.6(2)	91.7(1)	91.7(1)	92.2(1)	92.0(1)	92.2(1)
O(1A1)-Fe-O(2C1) × 2	92.9(2)	92.7(1)	92.5(1)	92.6(1)	92.1(1)	92.1(1)
O(1A1)-Fe-O(1B2) × 2	88.5(2)	88.6(1)	88.7(1)	88.6(1)	88.9(1)	88.9(1)
O(1A2)-Fe-O(2C1) × 2	87.6(2)	87.3(1)	87.4(1)	87.5(1)	87.2(1)	87.3(1)
O(1A2)-Fe-O(2D1) × 2	92.4(2)	92.4(1)	92.3(1)	91.8(1)	92.0(1)	91.7(1)
O(2C1)-Fe-O(2D1)	93.2(2)	93.3(1)	93.9(1)	94.2(1)	94.8(1)	95.1(1)
Volume	12.37(3)	12.25(2)	12.14(2)	12.02(2)	12.02(2)	11.90(2)
⟨λ⟩	1.0037(14)	1.0037(14)	1.0040(14)	1.0041(13)	1.0039(13)	1.0041(12)
σ²	12.30	12.23	13.19	13.54	13.02	13.42
			SiO₄tetrahedron			
SiO(1C1)	1.5769(43)	1.5734(37)	1.5824(37)	1.5827(36)	1.5751(34)	1.5744(31)
SiO(2C1)	1.5768(43)	1.5781(38)	1.5795(38)	1.5751(35)	1.5701(34)	1.5698(31)
Si-O(3C1)	1.6582(45)	1.6657(37)	1.6612(40)	1.6552(37)	1.6543(35)	1.6532(33)
Si-O(3C2)	1.6788(45)	1.6759(37)	1.6752(40)	1.6766(37)	1.6768(35)	1.6741(33)
Si-Si	3.0730(23)	3.0679(19)	3.0648(20)	3.0561(19)	3.0516(18)	3.0459(17)
O(1C1)-O(2C1)	2.6868(57)	2.6870(49)	2.6942(49)	2.6858(47)	2.6715(45)	2.6716(41)
O(1C1)-O(3C1)	2.6646(58)	2.6676(49)	2.6722(51)	2.6708(48)	2.6624(45)	2.6625(42)
O(1C1)-O(3C2)	2.6790(58)	2.6846(49)	2.6886(51)	2.6893(48)	2.6843(45)	2.6857(42)
O(2C1)-O(3C1)	2.6512(58)	2.6528(50)	2.6539(51)	2.6469(48)	2.6426(45)	2.6419(42)
O(2C1)-O(3C2)	2.5648(58)	2.5631(50)	2.5637(51)	2.5647(48)	2.5657(45)	2.5602(42)
O(3C1)-O(3C2)	2.6185(59)	2.6134(49)	2.6094(53)	2.6037(49)	2.6014(46)	2.5947(43)
O(1C1)-Si-O(2C1)	116.9(2)	117.0(2)	116.9(2)	116.5(2)	116.3(2)	116.4(2)
O(1C1)-Si-O(3C1)	110.9(2)	110.9(2)	110.9(2)	111.1(2)	111.0(2)	111.1(2)
O(1C1)-Si-O(3C2)	110.7(2)	111.4(2)	111.2(2)	111.2(2)	111.4(2)	111.5(2)
O(2C1)-Si-O(3C1)	110.1(2)	109.7(2)	109.9(2)	110.0(2)	110.1(2)	110.1(2)
O(2C1)-Si-O(3C2)	103.9(2)	103.9(2)	103.9(2)	104.1(2)	104.4(2)	104.2(2)
O(3C1)-Si-O(3C2)	103.4(2)	102.9(2)	102.9(2)	102.8(2)	102.7(2)	102.5(2)
Si-O3-Si	134.1(3)	133.3(2)	133.4(2)	133.1(2)	132.7(2)	132.5(2)
O3-O3-O3	161.8(2)	161.5(2)	161.2(2)	160.5(2)	159.9(2)	161.5(1)
Volume	2.175(8)	2.177(7)	2.182(8)	2.174(7)	2.161(7)	2.155(6)
[λ]	1.0061(34)	1.0065(30)	1.0064(30)	1.0063(29)	1.0061(27)	1.0064(25)
σ²	25.28	27.27	26.91	25.95	25.01	26.33
Tilting angle (°)*	2.19(11)	2.01(10)	2.14(10)	1.84(10)	1.56(9)	1.57(8)

Kandelin and Weidner 1988) shows that our values are up to 8% smaller (Table 6). Considering

$$K_S = K_T(1 + \alpha\gamma T) \qquad (4)$$

where α is the thermal expansion coefficient, γ the Grüneisen parameter, and T the temperature, the difference between K_T and K_S is about 2–3% for Ca-rich clinopyroxenes. At 298 K the K_{T_0} value of hedenbergite agrees well with the K_S value obtained from Brillouin experiments. Strictly speaking, our K_{T_0} values should be directly comparable to K_S derived by the Reuss averages because the latter values were obtained under conditions of ho-

mogeneous stress, which should apply also to our experimental conditions (Watt et al. 1976). Thus, our K_{T_0} values for both diopside and hedenbergite are in agreement with the Reuss averages within 2–3% after appropriate conversion using Equation 4 as shown in Table 7. Taking the anisotropic compression of the clinopyroxenes into account, it is not surprising that the difference between the Reuss and Voigt averages are indeed significant. From this point of view the K_{T_0} and K'_{T_0} values of diopside and hedenbergite determined in this study should be considered as more reliable than previously published data. It is remarkable that our K_{T_0} and K'_{T_0} values for diopside are
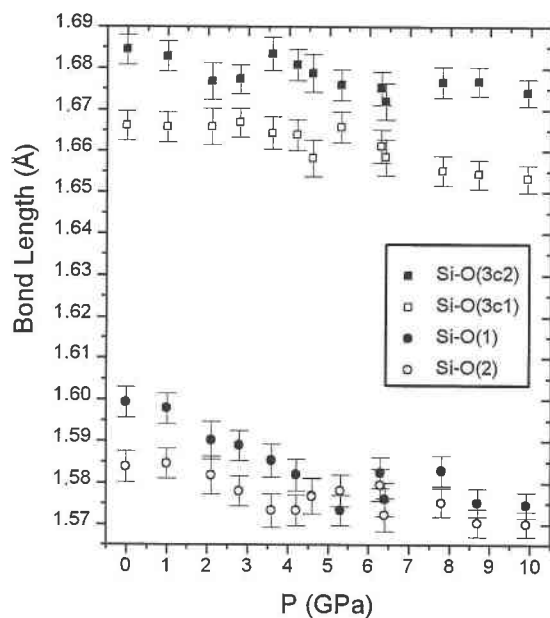
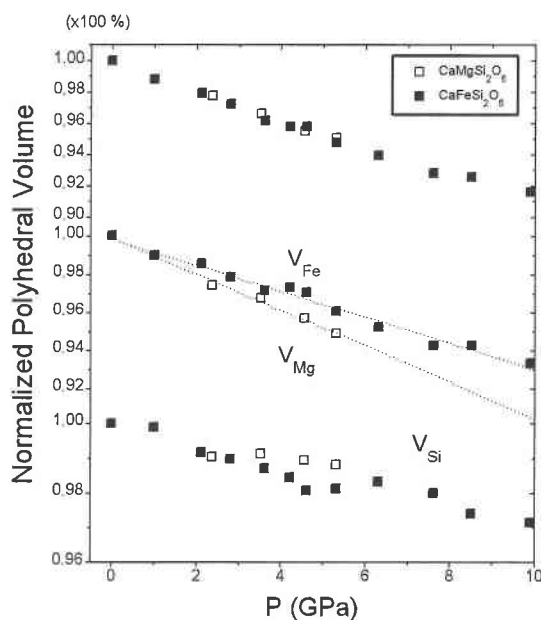**FIGURE 6.** Pressure dependence of Si-O interatomic distances in the SiO$_4$ tetrahedra.

FIGURE 7. Comparison of polyhedral compression in diopside and hedenbergite up to 5.3 GPa. The MgO$_6$ octahedra in diopside are about 1% more compressible than the FeO$_6$ octahedra in hedenbergite. The CaO$_8$ polyhedra and SiO$_4$ tetrahedra exhibit about the same compression in diopside as well as in hedenbergite.

practically identical with the values obtained from a theoretical calculation for simulated pressures up to 5 GPa (Matsui and Busing 1984).

Polyhedral compression in hedenbergite

The positional parameters of hedenbergite at 12 pressures are listed in Table 2. The interatomic distances (bond lengths) and bond angles as well as polyhedral volumes are presented in Table 8 and Figures 4, 5, and 6. The compressions among the bond lengths within the three polyhedra, CaO$_8$, FeO$_6$, and SiO$_4$, show significant anisotropy. To describe polyhedral geometry the nomenclature of Burnham et al. (1967) is used with M = Fe for M1 (point symmetry 2) and M = Ca for M2 (point symmetry 2).

CaO$_8$ polyhedron. There are four unique pairs of bond lengths. Between 0.1 MPa and 10 GPa, the longest bond pair, Ca-O(3C2,3D2), exhibits the highest compression of 6.9(2)%. The second longest bond pair, Ca-O(3C1,3D1), with a value 2.1(2)%, however, is not that with the second highest compression. The third longest bond pair, Ca-O(1A1,1B1), reveals a somewhat higher compression value of 2.3(3)%. The shortest bonds, Ca-O(2C2,2D2), are compressed the least: 1.3(3)%. The volume compression is 8.4%. This highly anisotropic behavior results in a crossover of the longest and the second longest bonds at about 4.5 GPa, where the lengths of two bond pairs apparently become the same. At about 10 GPa, the shortest and second shortest bond pairs merge together, becoming indistinguishable in length within the experimental error.

If the relative compressions of the individual bond lengths between 0.1 MPa and 10 GPa are normalized with

respect to the shortest polyhedral bond, the ratio 1:1.8:1.6:5.3 is obtained in the sequence for increasing bond length. Between 0.1 MPa and 5.3 GPa our data of hedenbergite can be compared with those for diopside (Levien and Prewitt 1981). The respective ratios for that range are 1:1.4:1.8:7.0 and 1:0.6:0.6:3.2. In both structures the longest bond pair shows the highest compression, whereas the values for the second and third longest pairs are quite similar. However, the shortest bond pair in hedenbergite is obviously compressed the least; this is not the case in diopside. Over this pressure range CaO$_8$ in hedenbergite has a volume compression of 5.3%, which is comparable to that of diopside: 5%.

FeO$_6$ octahedron. The three bond pairs of the FeO$_6$ octahedron display anisotropic compression. Between 0.1 MPa and 10 GPa, the longest bond pair, Fe-O(1A1,1B1), compresses by 3.1(3)%, the second longest pair, Fe-O(1A2,1B2), by 1.4(3)%, and the shortest pair, Fe-O(2C1,2D1), by 2.3(3)%. The volume compression is 6.6(3)%. Comparing bond compression in our hedenbergite and that in diopside between 0.1 MPa and 5.3 GPa, slightly smaller values are observed for all three bond pairs in hedenbergite. The respective values are 1.7(3), 0.8(3), and 1.6(3)% in the former and 2.1, 1.2 and 2.0% in the latter. The respective volume compressions are 4.0(4)% and 5% (Fig. 7). Thus, the MgO$_6$ octahedron is more compressible than FeO$_6$. As in CaO$_8$ a crossover of the longest and second longest bond pairs is observed at about 4.5 GPa. At pressures higher than 4.5 GPa, the

Fe-O(1A1,1B1) pair is significantly shorter than the Fe-O(1A2, 1B2) pair (Fig. 5).

SiO$_4$ tetrahedron. Significant anisotropic compression between 0.1 MPa and 10 GPa was also found in SiO$_4$ tetrahedra for all four bond lengths (Fig. 6). Unlike CaO$_8$ and FeO$_6$, the longest, Si-O(3C2), is not the most compressible one. The longest, Si-O(3C2), and second longest, Si-O(3C1) bonds compress only by 0.6(4)% and 0.8(4)%, respectively, whereas the values for the shortest, Si-O(2C1), and second shortest, Si-O(1C1), bonds are 0.9(4)% and 1.6(4)%, respectively. It is interesting to note that compression of the latter two bonds occurs mainly between 0.1 MPa and 4.5 GPa. At higher pressures the lengths of these two bonds are virtually the same within the experimental error. Moreover they become apparently insensitive to pressure. The volume compression between 0.1 MPa and 10 GPa is 2.9(6)%.

Several previous studies, especially that of orthoenstatite up to 2.1 GPa (Ralph and Ghose 1980), orthoenstatite up to 8 GPa (Hugh-Jones and Angel 1994), fassaite up to 5.2 GPa (Hazen and Finger 1977), and diopside up to 5.3 GPa (Levien and Prewitt 1981), implied that the Si-O bonds are quite incompressible below 4 GPa, but they indicated considerable shortening above 4 GPa (Hugh-Jones and Angel 1994). Our results demonstrate remarkable compressions of the Si-O1 and Si-O2 bonds even at relatively low pressures. The respective values are 1.1(5)% and 0.7(5)% between 0.1 MPa and 4.2 GPa. This can be visualized by looking at the volume data. For example, there is a volume compression of 1.6% from 0.1 MPa to 4.2 GPa that can be attributed mainly to the shortening of the two shortest Si-O bond, whereas there is only a reduction of 1.3% in SiO$_4$ volume from 4.2 to 9.9 GPa, resulting primarily from shortening of the two longest bonds. The volume compressibilities of SiO$_4$ in the lower and the higher pressure ranges are comparable: 3.7(8) × 10^{-3} GPa^{-1} and 2.3(5) × 10^{-3} GPa^{-1}, respectively. These new results indicate that at high pressure SiO$_4$ behaves like other polyhedra such as CaO$_8$ and FeO$_6$ in the structure. This was not observed in diopside (Levien and Prewitt 1981). Comparing the few high-pressure structure data measured well above 5 GPa, the average SiO$_4$ compressibility of 2.9(3) × 10^{-3} GPa^{-1} in hedenbergite between 0.1 MPa and 10 GPa is obviously smaller than, e.g., 6.2(1) × 10^{-3} in orthoenstatite, 7.1(3) × 10^{-3} in forsterite and 5.0(4) × 10^{-3} GPa^{-1} in andradite (Hugh-Jones and Angel 1994, and references therein).

The kinking angle of tetrahedral chains in silicates may be described by the O3-O3-O3 angle. The tilting angle of tetrahedra can be defined by the angle between the basal plane of a tetrahedron and the (100) plane. We observed a continuous kinking of this angle by 4.4° [2.7(2)%] as well as a continuous decrease of tetrahedral tilting with increasing pressure. This change is accompanied by a rotation of the SiO$_4$ tetrahedron around the normal to the tetrahedral basal plane.

DISCUSSION

Compression mechanism

The anisotropic unit-cell compression of Ca-rich clinopyroxenes may be generally accounted for by their constituent polyhedra, polyhedral linkages, and the bonding of atoms. The CaO$_8$ and (Fe,Mg)O$_6$ polyhedra build up a two-dimensional sheet in the b-c plane sandwiched by tetrahedral chains. This sheet actually possesses no rotational freedom. In fact the unit-cell compression is due mainly to the reduction of polyhedral volume. The sandwich sheet of CaO$_8$, FeO$_6$, and the SiO$_4$ chains are expected to be essentially resistant to compression along the a axis. Along the c axis, the tetrahedral chain has a relatively large rotational freedom through the corner-sharing tetrahedra that is described by the O3-O3-O3 angle. This rotational freedom of SiO$_4$ facilitates the compression in the c axis direction although the volume compression of tetrahedra is small. In addition, the compression of (Mg,Fe)O$_6$ and CaO$_8$ also contribute to the axial compression along the c axis. It is obvious that the relatively long Ca-O bonds projected into the b axis could account above all for the large compression in that direction.

The longitudinal elastic moduli, c_{11}, c_{22}, c_{33}, for diopside (223, 171, and 235 GPa) and hedenbergite (222, 176, and 249 GPa), determined by Brillouin spectroscopy at ambient conditions (Levien et al. 1979; Kandelin and Weidner 1988), are closely related to the compressibilities along the a, b, and c axes. Consistent with the above analysis, c_{22} is smallest for both diopside and hedenbergite. It should, however, be noted that c_{11} and c_{33} are about equal, with c_{33} being the largest. This disagrees with our high-pressure results, which show that compression along the a axis is the smallest. From the results of X-ray diffraction c_{11} should be the largest among the three longitudinal elastic moduli c_{11}, c_{22}, c_{33}. Furthermore, the similar magnitudes of c_{11} for diopside and hedenbergite contrast with their distinct a-axis compressibilities found in this study.

The CaO$_8$ polyhedra, FeO$_6$ octahedra, and SiO$_4$ tetrahedra constitute about 38% of the unit-cell volume. Compression of the cation polyhedra is 7.3% and that of voids 6.7%. Thus the unit-cell compression can be accounted for, to a large extent, by the compression of the constituent polyhedra. Based on the fact that the elastic coefficients c_{11} measured for diopside and hedenbergite are practically identical, and these parameters are different in orthoferrosilite and orthoenstatite, it was concluded (Kandelin and Weidner 1988; Bhagat and Bass 1992) that CaO$_8$ polyhedra determine the structural strength of Ca-rich clinopyroxenes. From our present results the compressibilities along the a axes of diopside and hedenbergite differ by as much as 20% over a wide pressure range. At pressures lower than 3 GPa this difference can be more than 50% (Fig. 8). Up to 10 GPa the CaO$_8$ polyhedron has an average bulk modulus of 118(3) GPa, FeO$_6$ octahedron 149(4) GPa, and SiO$_4$ tetrahedron 347(36) GPa, whereas the bulk modulus of all cation poly-
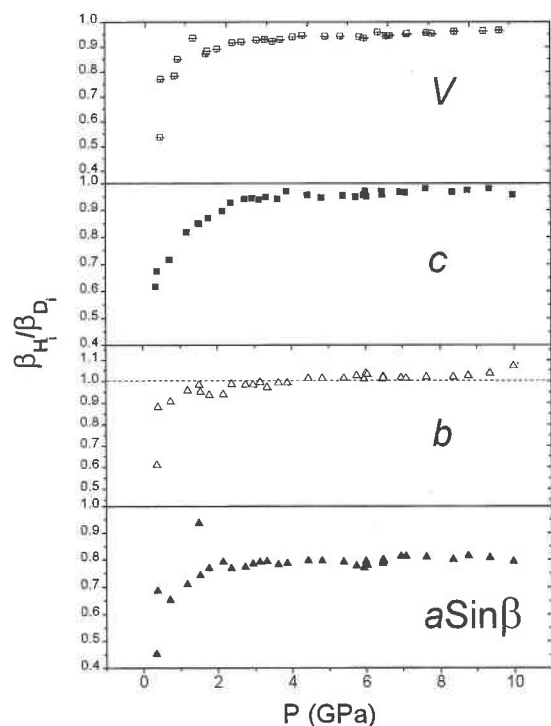
FIGURE 8. Comparison of axial and volume compressibilities between hedenbergite and diopside. The ratios of the compressibilities are plotted.

hedra is 136 GPa, which is just about the average of the bulk moduli of CaO_8 and FeO_6. Thus, from these two observations, we conclude that the compression of Ca-rich clinopyroxenes is determined mainly by both the CaO_8 and FeO_6 polyhedra. It is the distortion of these polyhedra, through their anisotropic compressions in bond lengths, that contributes mainly to the unit-cell compression. The compression of the SiO_4 tetrahedra plays a marginal role.

Influence of Fe,Mg substitution on elasticity and structural compression

The dependence of bulk modulus on Fe and Mg in mantle minerals is interesting for modeling the mineralogical composition of the mantle as well as for high-pressure crystal chemistry. Our experimental results on Ca-rich clinopyroxenes show clearly that K'_{T_0} of diopside is larger than that of hedenbergite, i.e., in the pressure range between 0.1 MPa and 10 GPa, diopside is about 10% more compressible than hedenbergite. This result is inconsistent with the predictions of the bulk modulus–volume systematics and provides another example for compression anomalies in silicate minerals. Such behavior was also observed in silicate garnets and olivine (Zhang et al., unpublished data) as well as in Fe-Mg spinel solid solution (Hazen 1993).

The effect of the Fe/Mg ratio on the compressional behavior of diopside and hedenbergite can be further visualized by comparing the pressure dependence of their axial compressibilities in dependence of pressure (Fig. 8). It is immediately clear that diopside shows significantly higher compressibilities in all axial directions at pressures below 3 GPa. Parallel to the b and c axes the compressibilities of both minerals approach each other with rising pressure. In the a^* direction diopside is about 20% more compressible than hedenbergite up to 10 GPa. This feature can be unambiguously attributed to the substitution of Mg for Fe^{2+} in the octahedra. The difference in the compression of these two minerals at high pressures is characterized by this feature. Because the high pressure data for diopside include a few data points only and are limited to 5.3 GPa (Levien and Prewitt 1981), it is difficult to explain this difference in terms of the individual bond lengths.

From the results of ^{57}Fe γ resonance on a Ca-rich clinopyroxene solid solution, Zhang and Hafner (1992) concluded that even at ambient conditions the Fe^{2+} and Mg cations in crystallographically equivalent octahedra must assume somewhat different geometric configurations. This may become more pronounced at high pressures. It implies that in solid solutions with similar cation compositions, Fe^{2+} and Mg occupancies could show increasing instability at mantle pressures. Our present results confirm that. In fact significant $Mg-Fe^{2+}$ ordering was observed in high pressure mantle minerals such as olivine and wadsleyite (Aikawa et al. 1985; Finger et al. 1993). The preferential participation of Fe^{2+} in oxide and Mg in perovskite in the lower mantle, following transformation from spinel $(Mg,Fe)_2SiO_4$ at about 670 km depth, could be explained by the distinct crystal chemical behavior of Fe^{2+} and Mg at high pressures as observed in this study.

Polyhedral distortion in hedenbergite

From the anisotrospic compression of bond lengths and bond angles in hedenbergite it is expected that the degree of polyhedral distortion changes with increasing pressure. For testing this, distortion parameters defined by Baur (1974) and Robinson et al. (1971) were used: bond length distortion (BLD), angle distortion (AD), edge-length distortion (ELD), quadratic elongation, $<\lambda>$, and angle variance, σ^2. The BLD, AD, and ELD values are plotted in Figure 9. The $<\lambda>$ and σ^2 values are given in Table 8. Within the error there is no significant change in $<\lambda>$ and σ^2 values for FeO_6 and SiO_4 for pressures up to 10 GPa. By examining the distortion parameters BLD, AD, and ELD for CaO_8, FeO_6, and SiO_4, it is evident that the distortion for CaO_8 decreases significantly with increasing pressure, whereas the other polyhedral distortion parameters show only marginal changes. Zhang and Hafner (1992) concluded that the geometry of FeO_6 becomes more regular with increasing pressure up to about 4 GPa on the basis of the ^{57}Fe data up to 10 GPa and by assuming a pseudoaxial symmetry at Fe^{2+} in hedenbergite. This trend seems to be confirmed by angle and edge distortion parameters of the FeO_6, which decrease slightly with increasing pressure. The cation off-center shifts in the CaO_8
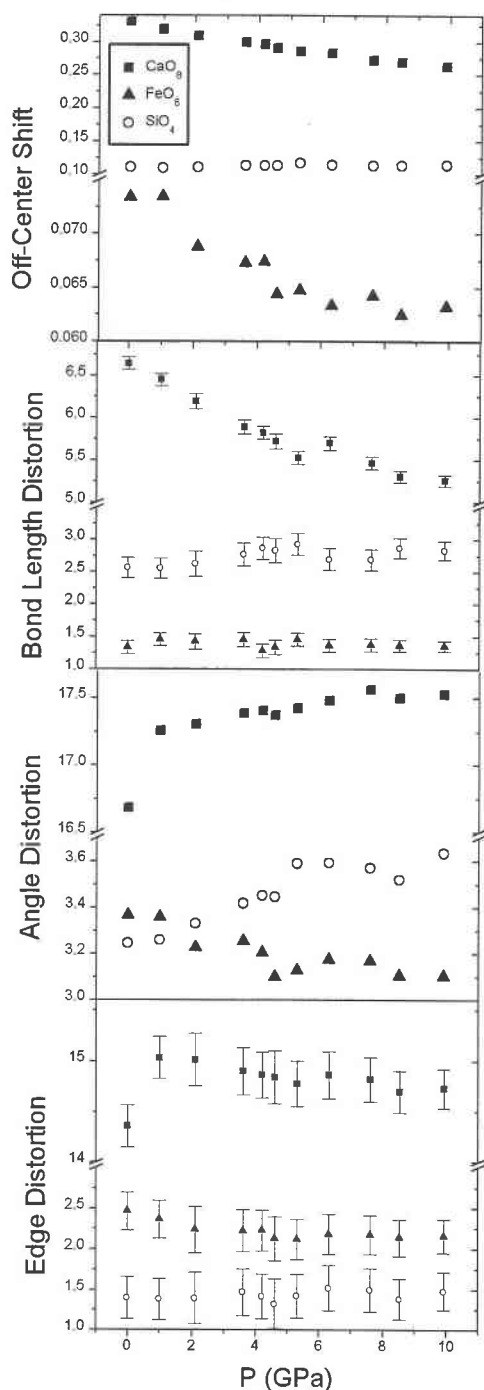
FIGURE 9. Distortion parameters and cation off-center shifts for CaO_8, FeO_6, and SiO_4. For a regular polyhedron the distortion parameters BLD, AD, and ELD are equal to zero.

Phase transition in hedenbergite

Recent studies of the ^{57}Fe γ (Mössbauer) resonance in three Ca-rich clinopyroxenes up to 10 GPa revealed a discontinuity in the electronic configuration of the Fe^{2+} ion at about 4 GPa, which may suggest a phase transition (Zhang and Hafner 1992). As demonstrated by the present results, neither any significant discontinuity in the unit-cell parameters nor any abrupt change in bond lengths or angles was observed within the experimental error in our X-ray diffraction study. The relatively large scatter of our data for the bond lengths and bond angles in FeO_6 does not allow detection of any such small discontinuity required for a change in Fe^{2+} electronic state. Although the ^{57}Fe hyperfine parameters are critically dependent on the local geometry of the FeO_6 octahedra it is not yet clear how these parameters relate to that state. However, it is interesting to note that the discontinuity in hyperfine parameters of Fe^{2+} coincides with the crossover of the two longest bond lengths in both the CaO_8 and FeO_6 polyhedra at about 4 GPa. Furthermore, there is a change in the compressibilities of the two shortest bond lengths in the SiO_4 tetrahedron at about 4 GPa. No reflections violating space group $C2/c$ were detected above 4 GPa.

Diopside and hedenbergite undergo twining at nonhydrostatic pressures even in a pressure transmitting medium of solid argon. This behavior was tested by using methanol-ethanol, solid argon, and teflon oil as pressure-transmitting media. No twinning could be observed in the methanol-ethanol medium up to 10 GPa. Twinning was observed in the crystals in the argon pressure medium beginning at about 3 GPa and persisting up to at least 15 GPa. The twining disappeared, however, after releasing pressure. In teflon oil the twinning started at much lower pressures and was retained after releasing pressure. Twinning of both diopside and hedenbergite is, as demonstrated here, clearly induced by deviatoric stresses. Although the high pressure Mössbauer experiments on Ca-rich clinopyroxenes were not conducted under hydrostatic conditions, twinning due to nonhydrostatic pressure would not change the hyperfine parameters measured from polycrystalline samples. Furthermore, the pressure of the hyperfine parameter discontinuity was found to be much higher than that needed for twinning, even if compared with the pressure in the argon medium. Considering that the Mössbauer experiment probes the Fe^{2+} electronic state in the FeO_6 octahedron with much more sensitivity than X-ray diffraction, it seems inevitable that more precise structure data on diopside and hedenbergite will be needed to clarify this question.

and FeO_6 polyhedra, defined by the deviation of the average mass center of the ligands from the mass center of the cation in a polyhedron, decrease with increasing pressure, whereas the off-center shift for SiO_4 is unchanged with pressure.

References Cited

Ahsbahs, H. (1987) X-ray diffraction on single crystals at high pressure. Progress of Crystal Growth and Characterization, 14, 263–302.

Aikawa, N., Kumazawa, M., and Tokonami, M. (1985) Temperature dependence of intersite distribution of Mg and Fe in olivine and the associated change of lattice parameters. Physics and Chemistry of Minerals, 12, 1–8.

Aleksandrov, K.S., and Rythova, T.V. (1961) The elastic properties of rock forming minerals, pyroxenes and amphiboles. Bulletin of Academy of Sciences USSR, Geophysical Series, 871–875.

Anderson, D., and Bass, J.D. (1984) Composition of the upper mantle: Geophysical tests of two petrological models. Geophysical Research Letters, 11, 237–240.

Baur, W.H. (1974) The geometry of polyhedral distortions. Predictive relationships for the phosphate group. Acta Crystallographica, B30, 1195–1215.

Bhagat, S.S. and Bass, J.D. (1992) Single-crystal elastic properties of omphacite-C2/c by Brillouin spectroscopy. Journal of Geophysical Research, 97, 6843–6848.

Birch, F. (1978) Finite strain isotherm and velocities for single and polycrystalline NaCl at high pressures and 300 K. Journal of Geophysical Research, 83, 1257–1268.

Burnham, C.W., Clark, J.R., Papike, J.J., and Prewitt, C.T. (1967) A proposed crystallographic nomenclature for clinopyroxene structures. Zeitschrift für Kristallographie, 125, 1–6.

Cameron, M., Sueno, S., Prewitt, C.T., and Papike, J.J. (1973) High-temperature crystal chemistry of acmite, diopside, hedenbergite, jadeite, spodumene, and ureyite. American Mineralogist, 58, 594–618.

Comodi, P., Princivalle, F., Tirone, M., and Zanazzi, P.F. (1995) Comparative compressibility of clinopyroxenes from mantle nodules. European Journal of Mineralogy, 7, 141–149.

Finger, L.W., Hazen, R.M., Zhang, J., Ko, J., and Navrotsky, A. (1993) The effect of Fe on the crystal structure of wadsleyite β-(Mg$_{1-x}$Fe$_x$)$_2$SiO$_4$, $0.00 \le x \le 0.40$. Physics and Chemistry of Minerals, 19, 361–368.

Hazen, R.M. (1993) Comparative compressibilities of silicate spinels: anomalous behavior of (Mg,Fe)$_2$SiO$_4$. Science, 259, 206–209.

Hazen, R.M., and Finger, L.W. (1977) Compressibility and crystal structure of Angra dos Reis fassaite to 52 kbar. Carnegie Institution of Washington Year Book, 76, 512–515.

Hugh-Jones, D.A., and Angel, R.J. (1994) A compressional study of MgSiO3 orthoenstatite up to 8.5 GPa. American Mineralogist, 79, 405–410.

Ibers, J.A., and Hamilton, W.C., Eds. (1974) International tables for X-ray crystallography, vol. IV, 366 p. Kynoch, Birmingham, U.K.

Kandelin, J., and Weidner, D.J. (1988) Elastic properties of hedenbergite. Journal of Geophysical Research, 93, 1063–1072.

King, H., and Finger, L.W. (1979) Diffracted beam crystal centering and its application to high-pressure crystallography. Journal of Applied Crystallography, 12, 374–378.

Kutoglu, A. (1995) Crymis: a software package for structural analysis (Version 95). University of Marburg, Germany.

Lehmann, M.S., and Larsen, F.K. (1974) A method for location of the peak in step-scan-measured Bragg reflexions. Acta Crystallographica, A30, 580–584.

Levien, L., and Prewitt, C.T. (1981) High-pressure structural study of diopside. American Mineralogist, 66, 315–323.

Levien, L., Weidner, D.J., and C.T. Prewitt (1979) Elasticity of diopside. Physics and Chemistry of Minerals, 4, 105–113.

Loveday, J.S., McMahon, M.I., and Nelmes, R.J. (1990) The effect of diffraction by the diamond-anvil cell on single-crystal sample intensities. Journal of Applied Crystallography, 23, 392–396.

Matsui, M., and Busing, W.R. (1984) Calculation of the elastic constants and high-pressure properties of diopside, CaMgSi$_2$O$_6$. American Mineralogist, 69, 1090–1095.

McCormick, T.C., Hazen, R.M., and Angel, R.J. (1989) Compressibility of omphacite at 60 kbar: role of vacancies. American Mineralogist, 74, 1287–1292.

Munro, R.G., Piermarini, G.J., Block, S., and Holzapfel, W.B. (1985) Model line-shape analysis for the R lines used for pressure measurement. Journal of Applied Physics, 57, 165–169.

Ralph, R.L., and Ghose, S. (1980) Enstatite, Mg$_2$Si$_2$O$_6$: Compressibility and crystal structure at 21 kbar (abstract) EOS, 61, 409.

Ralph, R.L., and Finger, L.W. (1982) A computer program for refinement of crystal orientation matrix and lattice constants from diffractometer data with lattice symmetry constrains. Journal of Applied Crystallography, 15, 537–539.

Ringwood, A.E. (1975) Composition and petrology of the Earth's mantle, 618 p. McGraw-Hill, New York.

Robinson, K., Gibbs, G.V., and Ribbe, P.H. (1971) Quadratic elongation: A quantitative measure of distortion in coordinated polyhedra. Science, 172, 567–570.

Watt, J.P., Davies, G.F., and O'Connell, R.J. (1976) The elastic properties of composite materials. Review of Geophysics, 14, 541–563.

Zeug, J.M., Abramson, E.H., Brown, J.M., and Slutsky, L.J. (1993) Sound velocities in olivine at earth mantle pressures. Science, 260, 1487–1489.

Zhang, Li., Ahsbahs, H., Turk, P.-G., and Hafner S.S. (1989) A pressure induced phase transition in pyroxene. High Pressure Research, 733–735.

Zhang, Li., and Hafner, S.S. (1992) ^{57}Fe gamma resonance and X-ray diffraction studies of Ca(Fe,Mg)Si$_2$O$_6$ clinopyroxenes at high pressure. American Mineralogist, 77, 462–473.

Zhang, Li., and Chopelas, A. (1994) Sound velocity of Al$_2$O$_3$ to 616 kbar. Physics of Earth and Planetary Interiors, 87, 1-2, 77–83.